# Selective laser sintering of polymer biocomposites based on polymethyl methacrylate

Rajkumar Velu and Sarat Singamneni[a)]
*Department of Mechanical Engineering, School of Engineering, AUT University, Auckland 1010, New Zealand*

(Received 8 April 2014; accepted 22 July 2014)

Materials and processes used for medical applications should have specific attributes. For bone repair and reconstruction, controlled open porosity and osteoconductivity are essential apart from mechanical strength and biocompatibility. Several forms of calcium phosphates are often used for these applications, considering properties similar to bone minerals, but often in combinations with other biopolymers. Polymethyl methacrylate (PMMA) and β-tricalcium phosphate (β-TCP) are identified as a suitable combination for the current research, considering specific properties both individually and in combinations, when processed by different means for specific medical applications. Specific responses of the biocomposite material formed by mechanically mixing the two materials in the powder form to selective laser sintering (SLS) under varying conditions are investigated. The results indicate the suitability of the material system for SLS, while controlled porosity and mechanical property combinations are possible by optimizing material composition and process parameters.

## I. INTRODUCTION

Ceramics and their composites are used for medical applications such as repair of bone fractures and attachment of bone plates, apart from being substitute materials in dental and orthopedic requirements.[1,2] The material used as a bone substitute should be biocompatible, easily available, and easy to process, apart from having the compressive strength necessary to serve as the base material for new bone growth. While ideal material systems are yet to evolve, porous ceramics based on calcium phosphate possess properties similar to bone minerals and exhibit unique characteristics as bone substitutes, compared to other biomaterials. They also induce biological responses during bone remodeling, involving the resorption of old bone minerals coupled with the formation of the new bone. During resorption, the degradation products of calcium phosphate bioceramics (calcium and phosphate ions) are naturally metabolized and they do not induce abnormal calcium or phosphate levels in the organs of the body.[3] The primary constitution of the natural bone includes 60% of calcium phosphate minerals and hence calcium phosphate has the osteoconductive property to be a bone substitute.[4] Calcium phosphates were shown to exhibit a variety of forms, but from the chemical point of view, hydroxyapatite (HA),[5] β-tricalcium phosphate (TCP),[6] multiphasic bioglass, biphasic calcium phosphate (BCP), and octacalcium phosphate (OCP) have evolved over time and have been investigated both in vitro and in vivo.[7]

Among these, TCP has better biodegradability and is most commonly used in bone surgery. It has two major distinct phases of anhydrous crystals: monoclinic α-TCP (low-temperature polymorph) and rhombohedral β-TCP (high-temperature polymorph). Further, considering better biocompatibility, osteoconductivity, and cell-mediated resorbability, β-TCP ($Ca_3(PO_4)_2$) and its derivatives and combinations are most commonly used as bone substitutes. The common Ca/P ratio of 1.5 is within the physiological range of the human bone, which is 1.3–1.66, depending on the person's age and state of well-being.[8] The most stable phase is β-TCP, up to 1125 °C, and so its thermal stability and transformation behavior are well under control. β-TCP possesses a high affinity for proteins and its porous structure acts as a filter to accumulate the growth factors from the surrounding body fluids. On implantation of β-TCP particles or porous blocks in the bone, new lamellar cancellous bone forms within 4–8 weeks. It is also noteworthy that β-TCP is resorbed by osteoclast cells, whereas the much slower resorption of hydroxyapatite is affected mainly by foreign-body giant cells with limited resorbability.

The processing methods often used with β-TCP are synthetic manufacturing approaches by mechanical–chemical means, but the mechanical strength and the fracture toughness are still low, restricting its use in low load-bearing applications.[9] Alternatively, these types of ceramics can also be processed together with certain biopolymer materials, targeting specific property improvements. The resulting synthetic polymers with

[a)]Address all correspondence to this author.
e-mail: sarat.singamneni@aut.ac.nz
DOI: 10.1557/jmr.2014.211

 © Materials Research Society 2014 

https://doi.org/10.1557/jmr.2014.211 Published online by Cambridge University Press

necessary biocompatibility, sterilizability, physical properties, and manufacturability are suitable for disposable medical supplies, prosthetics, dressings, extracorporeal devices, drug delivery systems, implants, and orthopedic and dental needs.[3,4]

While several polymer options were tried earlier in combination with TCP, polymethyl methacrylate (PMMA) ($C_5O_2H_8$) has been identified as a potential processing medium, considering its excellent compatibility with human tissue and suitability for medical implants. The interconnected porosity, bone on and in-growth characteristics, allow PMMA to be used as bone cement to fix implants and remodel lost bones.[9,10] A fully amorphous structure, together with thermoplastic behavior and easy and clean thermal elimination, are its critical attributes; the spherical shape of the PMMA pellets also allows the building of a frame with close and numerous contacts between particles and controls the dimension, the morphology, and the homogeneity of the compound.

To induce bone growth in a porous bioceramic, it is necessary to control the physical characteristics of the porosity of the implant.[11] While numerous methods have evolved to achieve macroporous structures, the most common approaches reported in the literature include the polymeric sponge method,[12] addition of porogen organic agents in the powder or the suspension,[13] and introduction of foaming agents into the ceramic slurry ($H_2O_2$, etc.).[14] However, limitations of these processes are well identified and include, for example, partial reproduction and nonhomogeneity of the structure, uncontrolled size and shape as well as interconnection between macropores, and poor mechanical properties.

Descamps et al.[15] developed PMMA and β-TCP composites by means of a thermal forming technique and evaluated the resulting macroporous structures. The mechanism of material consolidation involves a viscous flow and sintering of the PMMA coating over the relatively smaller TCP particles. While the control over the macroporosity was reported to be good, the dimensional stability was poor. When used for scaffolding, the resulting material structure should have specific attributes to match with the material properties of the native bone tissue and also allow for the sequential growth of the neotissue as the scaffold degrades with time. While several novel materials and processing techniques were investigated to address these requirements,[16] the search for better alternatives continues and current research looks at the possibility of processing the PMMA and β-TCP composites using an additive manufacturing process.

With some recent developments, certain rapid prototyping technologies have evolved as possible means of achieving the required critical process and product attributes for medical requirements with biomaterials.[17,18] The layer-by-layer manufacturing methods (known as additive manufacturing), encompass different technologies offering certain unique characteristics for the end product, including unlimited design freedom and control over the macrostructures, where necessary. Specifically, selective laser sintering (SLS) scores the best in terms of processing biopolymers in powder form.[19,20] A $CO_2$ laser is commonly used considering the laser absorptivities of polymeric materials, and the powder material is converted into 3D forms based on raster path data generated from CAD files. With polymer/ceramic composites, it is the low melting polymer that melts with laser sintering and forms the matrix to support the functional ceramic. The interconnected porosity can be controlled through material selection, physical design, and processing parameters.[21]

SLS applications in biomaterials were mainly attempted for developing scaffold structures in tissue engineering. Williams et al.[22] used SLS to process polycaprolactone to produce parts with controlled pore sizes in the range 1.75–2.5 mm and designed porosities from 63.1% to 79%, but met with limited success in terms of accurately achieving the required porosity levels. Particle size and thermodynamic variations were found to play critical roles. Tan et al.[23] and Chua et al.[24] demonstrated the ability of SLS to fabricate physically blended hydroxyapatite (HA)–poly (ether–ether–ketone) (PEEK) and HA–poly (vinyl alcohol) composites for tissue scaffold development and observed micropores on the scaffold surface. Das et al.[25] investigated the production of HA–poly-(l-lactic acid) (PLLA) parts by SLS and noted the ultimate compressive strength and elastic modulus to be in the lower limits of reported values for cancellous bone. During the early stages, application of laser sintering to fabricate implants with composites of HA and β-TCP materials[26] involved coating, reinforcing, and blending of the ceramic powder with a secondary polymeric binder. Evidently, there were some attempts toward the application of SLS of composites of both HA and TCP with a few other polymers,[23,24,27] but the PMMA and β-TCP composites were not investigated yet for SLS. The current research attempts this through initial experiments evaluating the basic material responses and further experimental investigations leading to an understanding of the influences of critical process parameters.

## II. EXPERIMENTAL METHODOLOGY

### A. Materials

The PMMA and β-TCP composites are candidate materials for the SLS experiments conducted as part of this research. The primary aim is to establish the material response to processing by SLS, but typical relationships between critical process parameters and specific

https://doi.org/10.1557/jmr.2014.211 Published online by Cambridge University Press

responses are also investigated. The PMMA powder was supplied by Aldrich chemicals with an average particle size of 75 μm. The melting and the glass transition temperatures are 160 °C and 106 °C respectively and the theoretical density that can be achieved is 1180 kg/m$^3$. The β-TCP powder material was supplied by May & Baker Ltd., Dagenham, England, and has a relative density of 3180 kg/m$^3$. Two blend compositions are developed by mixing PMMA with 10% and 20% β-TCP; the scanning electron microscopy (SEM) photographs of the green powders are shown in Fig. 1. The larger grains represent the PMMA spheres, while the finer particles are that of β-TCP and the green powder is a simple mixture of the two different powder particles, with no further interactions.

### B. SLS experimental system and processing

In SLS, a laser beam scans the powder bed in a series of strokes referred to as the raster patterns to partially or fully melt the substrate particles and promote interparticle fusion, sintering, and subsequent integration. Three critical parameters arise out of this mechanism: laser power ($P$), scan speed ($v$), and beam diameter ($D$). A makeshift SLS system is designed and built using an off-the-shelf 60 W $CO_2$ laser that can provide an average power output ranging from 0.6 to 60 W and scan speeds up to 5000 mm/s. A manual powder dispersion method is used to produce test samples with varying process conditions. The $CO_2$ laser with a 10.6 μm wave length is suitable for sintering PMMA powders, in terms of the laser absorptivity aspect. The spot size and focal length of the laser are 540 μm and 370 mm respectively and a computer-controlled optical deflection system allowed the desired raster scan patterns to be achieved. An electrically heated aluminum base plate is used as the substrate surface to maintain the powder bed at around 100 °C, slightly below the glass transition temperature of PMMA.

The energy density (ED) per unit area along the scan line can be evaluated as

$$\mathrm{ED}\ (\mathrm{J/mm^2}) = P/(D^{*}v) \quad , \qquad (1)$$

where $P$ is the laser power, $D$ is the beam diameter, and $v$ is the scan velocity.

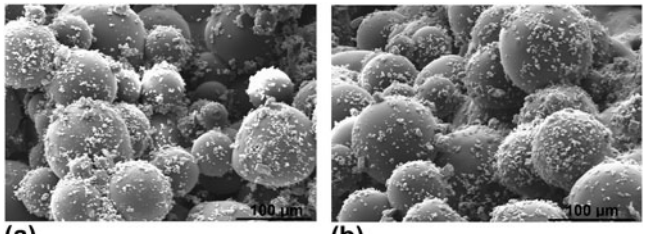



FIG. 1. SEM micrograph of PMMA powders mixed with (a) 10% and (b) 20% β-TCP.

Initial experiments involving single-layer sintered samples have been designed mainly to understand the effects of the critical process parameters on the interparticle coalescence and the overall consolidation of the powder material in a single layer. Samples are produced with varying process parameters and the resulting layer thicknesses are established through micrometer measurements. The particle dispersion, surface morphologies of the sintered single layers, and the cross-sections of the scalpel-cut sintered blocks are examined using a SEM examination of samples sputter coated with gold prior to imaging. The data generated from the initial experiments are used to further enhance the process conditions.

## III. INITIAL EXPERIMENTS AND RESULTS

Single-layer test samples are produced from the initial experiments by varying the laser power in the range 13–24 W and scan velocities from 250 to 500 mm/s, respectively. SEM photographs are generated based on the single-layer samples to understand the interparticle bonding and melt-flow behavior with varying process parameters. Variation in the density of pores as observed from the SEM photographs is used to evaluate the surface morphologies. While both blends of the composite are successfully sintered, the laser power and the scan speed are found to play significant roles, apart from the composition of the composite material. Alessandro and Luca[28] studied the sintering depth and height of polyamide and phenolic-coated sand following single-pass laser scanning and showed that appropriate energy densities have to be used for proper sintering. Williams and Dechard[29] investigated the height and depth of the single-pass sintered powders and ascertained that a certain minimum power is indispensable to induce sintering, while laser scan speeds exceeding certain limits result in poor sintering.

SEM photographs of single-layer samples produced using a 10% TCP + PMMA composite with the laser power fixed at 22.8 W and varying scan speed settings are shown in Fig. 2. The effects of varying scan speeds are similar to observations made by Williams and Dechard,[29] indicating very poor interparticle coalescence at higher speeds as evident from the coarse structure in Fig. 2(a). When the scan speed is reduced to 381 and 254 mm/s, improved interparticle coalescence is observed in the base matrix material, clearly elucidating the role of sintering time in achieving sufficient interparticle coalescence. Further trials clearly indicate a gradual improvement with increasing power, with each speed setting, as the samples show wider areas of the PMMA powder sufficiently coalesced to form continuous networks of the matrix holding the β-TCP particles. Again,

https://doi.org/10.1557/jmr.2014.211 Published online by Cambridge University Press

at any given speed, the base polymer degrades and disintegrates when the power is increased beyond a certain limit. Considering the three cases presented in Fig. 2, there is a gradual improvement from case (a) to case (c), while the sample with the lowest speed of 254 mm/s exhibited the best results with the PMMA phase coalesced significantly over wide areas. It is also evident that the optimum combination of laser power and scan speed are beyond the limits of these initial trials.

The thickness of the sintered layer also varies with laser power and scan speed settings. The variation of the thickness of single sintered layers is assessed with varying laser power and the scan speed set at 381 mm/s, and the results are as shown in Fig. 3(a). The thickness of the sintered layer increased with increasing laser power, as the absorption increases, resulting in a wider sintered zone. It was observed that the interroad coalescence was poor below 13 W, but the sintering results are good and the layer formation is uniform with laser power varying between 13 and 35 W. Beyond 35 W, however, the material begins to char, discolor, and degrade; emanates smoke; and results in a disintegrated layer. Evidently, the process works only within certain ranges of constituent parameters. The effects of varying the laser scan speed at two different laser power settings on the thickness of sintered samples are depicted in Fig. 3(b). Again the effective energy absorption control the layer thickness, as increasing speed results in decreasing layer thickness for any given power. It may be observed that the layer thickness stabilizes at around 500 μm when the scan speed increases beyond a certain value in both cases. While the layer thickness is a function of the rate of energy flow into the substrate,[30] for the powder particle size and the relatively high power setting used, the layer thickness obtained is constant above the critical speed levels, within the speed limits shown in Fig. 3(b). However, it must be noted that the layer thickness will drop first and then lead to insufficient sintering, if the scan speeds are increased beyond these limits.

Interestingly, the process attributes completely changed, with the following material composition: 80% PMMA + 20% β-TCP. Figure 4 presents the SEM photographs of single-layer samples produced with 18 W power and two different speed settings. It may be noted that the laser-sintering behavior of the material changed entirely with the increased amount of β-TCP. Though there is a certain improvement in the coalesced state from the higher scan speed case as shown in Fig. 4(a) to the lower scan speed case presented in Fig. 4(b), in general, the material response to sintering is poor, perhaps due to the rheological changes of the PMMA with increased β-TCP content. With any given speed, the material shows signs of degrading and decolorization when the laser power is increased beyond 18 W. Probably the thermodynamics of the process is altered because of the excessive presence of the β-TCP phase, in terms of higher energy absorption as the laser scans a given point and subsequently dissipates the same, resulting in the overheating and degrading of the surrounding matrix phase.

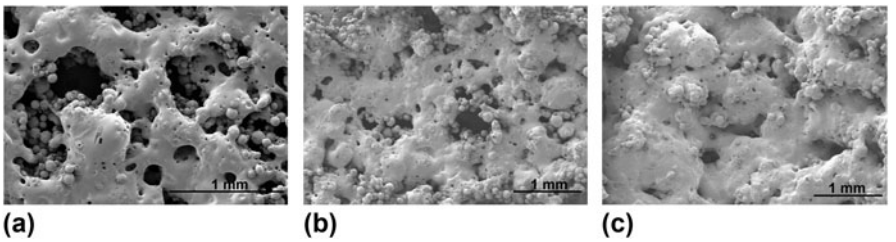



FIG. 2. SEM photographs of the sintered single layer with PMMA 10% TCP composite with laser power of 22.8 W and varying scan speeds (a) $s$ = 508 mm/s; (b) $s$ = 381 mm/s; (c) $s$ = 254 mm/s.

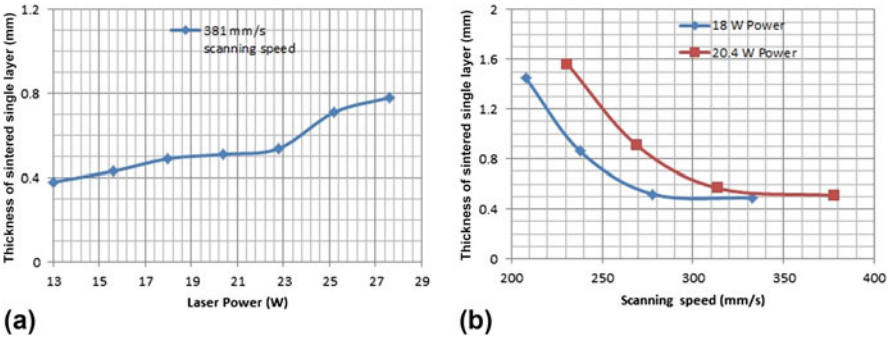



FIG. 3. Effects of process parameters (a) laser power and (b) laser scan speed on critical responses (10% TCP composite powder).

https://doi.org/10.1557/jmr.2014.211 Published online by Cambridge University Press

## IV. FURTHER EXPERIMENTAL TRIALS AND SURFACE MORPHOLOGIES

Based on the initial results, further experimental trials are designed taking into account laser power and scan speed settings closer to the optimum levels. Considering test cases with relatively better sintering results from Fig. 2, together with the ED calculations based on Eq. (1), four ED levels are identified as possible conditions for achieving better sintering. Table I lists the ED levels identified as the most suitable settings for the PMMA composite with 10% β-TCP. Keeping the effective energy densities at these four levels, several combinations of laser scan speed and power settings varying within relatively narrow ranges are identified as given in Table I. Experiments are conducted with these parameter settings producing single-layer samples, and SEM photographs of the surface morphologies of selected samples are shown in Fig. 5. It is generally observed that all three samples showed similar levels of coalescence and consolidation of the PMMA powder within any given ED level. However, there is a gradual improvement with each power setting as the scan speed is reduced. Overall, the ED levels 0.14 and 0.16 J/mm$^2$ appear to give better sintering results. It was also noted that partial melting partial neck formation are noted with the power set below 18 W, while complete fusion made the boundaries of particles indistinguishable when the power used is above 18 W, with any of the ED settings used. Porosity is observed in all samples, but with the intensities decreasing with increased coalescence across the thin layer.

With ED set at 0.16 J/mm$^2$, the particles are sufficiently fused and the normal pore size decreased considerably, indicating significant melting and subsequent interparticle coalescence and bonding. However, large voids are randomly created probably due to the presence of the β-TCP particles increasing the viscosity of the melt pool as well as offering resistance to the melt flow. Rimell and Marquis[31] observed that with still higher laser power settings, the polymer substrate is likely to go through a physical breakdown of polymer chains, resulting in a lighter material which eventually vaporizes.

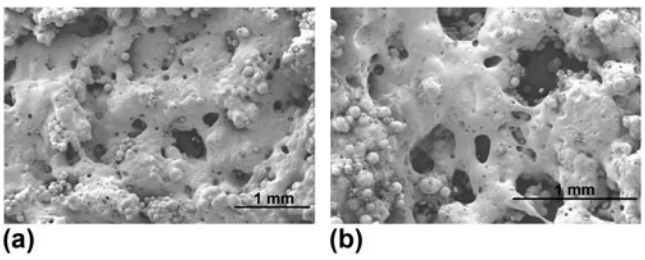



FIG. 4. SEM photographs of the sintered single layer with PMMA + 20% β-TCP composite powders. (a) $P$ = 18 W, $s$ = 508 mm/s; (b) $P$ = 18 W, $s$ = 254 mm/s.

TABLE I. Experimental condition with specific energy densities and general observations.

| Energy density (J/mm$^2$) | Laser power (W) | Scan speed (mm/s) |
|---|---|---|
| | 18 | 333 |
| 0.1 | 20.4 | 378 |
| | 22.8 | 422 |
| | 18 | 278 |
| 0.12 | 20.4 | 315 |
| | 22.8 | 352 |
| | 18 | 238 |
| 0.14 | 20.4 | 269 |
| | 22.8 | 300 |
| | 18 | 208 |
| 0.16 | 20.4 | 231 |
| | 22.8 | 263 |

## V. EVALUATION OF INFLUENCES OF CRITICAL PROCESS PARAMETERS

Considering the improvements evident as the laser power is increased with ED values at 0.1, 0.12, 0.14, and 0.16 J/mm$^2$, further sintering trials are conducted by shifting the laser power settings to the range 37–42 W, as listed in Table II. SEM photographs of the single-layer samples produced with the modified conditions are presented in Fig. 6. A careful observation of the photomicrographs of Fig. 6 reveals that with ED equal to 0.1 J/mm$^2$, lower power values resulted in better sintered structure. However, with the other two ED settings of 0.12 and 0.14 J/mm$^2$, the higher the power, the better is the sintering. Further, considering the three photographs of the third column, for the same power setting of 42 W, the best sintering result is obtained with scan speeds in the

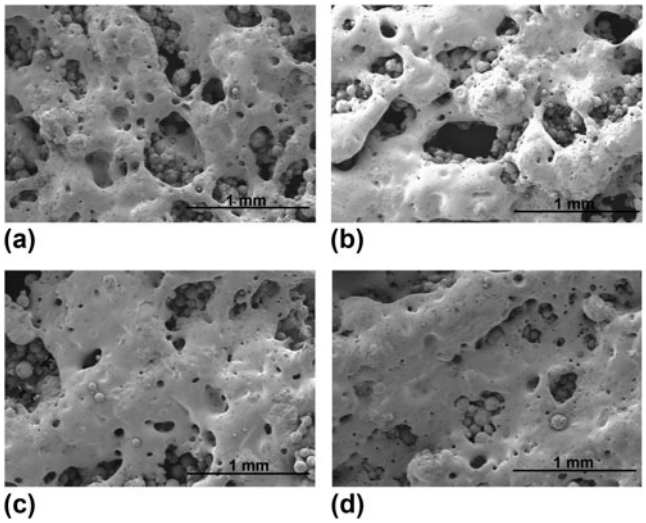



FIG. 5. SEM photographs of sintered PMMA–β-TCP composite single layer samples with varying EDs, laser power, and scan speed. (a) ED = 0.1 J/mm$^2$, $P$ = 22.8 W, $s$ = 422.17 mm/s; (b) ED = 0.12 J/mm$^2$, $P$ = 22.8 W, $s$ = 352 mm/s; (c) ED = 0.14 J/mm$^2$, $P$ = 22.8 W, $s$ = 300 mm/s; (d) ED = 0.16 J/mm$^2$, $P$ = 22.8 W, $s$ = 263 mm/s.

https://doi.org/10.1557/jmr.2014.211 Published online by Cambridge University Press

midranges. But overheating and rapid degradation of the powder bed occurred when the laser power is increased beyond 37 W for ED of 0.16 J/mm$^2$ and 42 W for ED of 0.14 J/mm$^2$.

Ideally, scaffolds must possess an interconnected open-pore geometry and microstructure, permitting cell in-growth and reorganization during the in vitro phase, providing the necessary space for neovascularization from the surrounding tissues.[32] Evidently, the porosity levels of all sintered test pieces varied with laser power and scan speed settings implying that the porosity of the β-TCP + PMMA composite parts can be controlled by using appropriate energy settings while achieving the necessary mechanical properties. A number of other parameters such as scan space, scan pattern, beam spot size, and layer thickness may also control the porosity levels in sintered specimens of the composite material, as these parameters will also influence the energy imparted to the powder surface as also observed with other material systems.[33]

However, uncontrolled porosity is also possible under certain conditions. First, inadequate energy levels resulting from either too low power or too high scan speed settings may lead to poor interparticle coalescence and, consequently, sparsely connected grain structures, resulting in

TABLE II. Surface morphologies of single-layer samples sintered with higher power settings.

| Energy density (J/mm$^2$) | Laser power (W) | Scan speed (mm/s) |
|---|---|---|
| | 37.2 | 711 |
| 0.1 | 39.6 | 762 |
| | 42 | 812 |
| | 37.2 | 635 |
| 0.12 | 39.6 | 655 |
| | 42 | 736 |
| | 37.2 | 457 |
| 0.14 | 39.6 | 482 |
| | 42 | 508 |

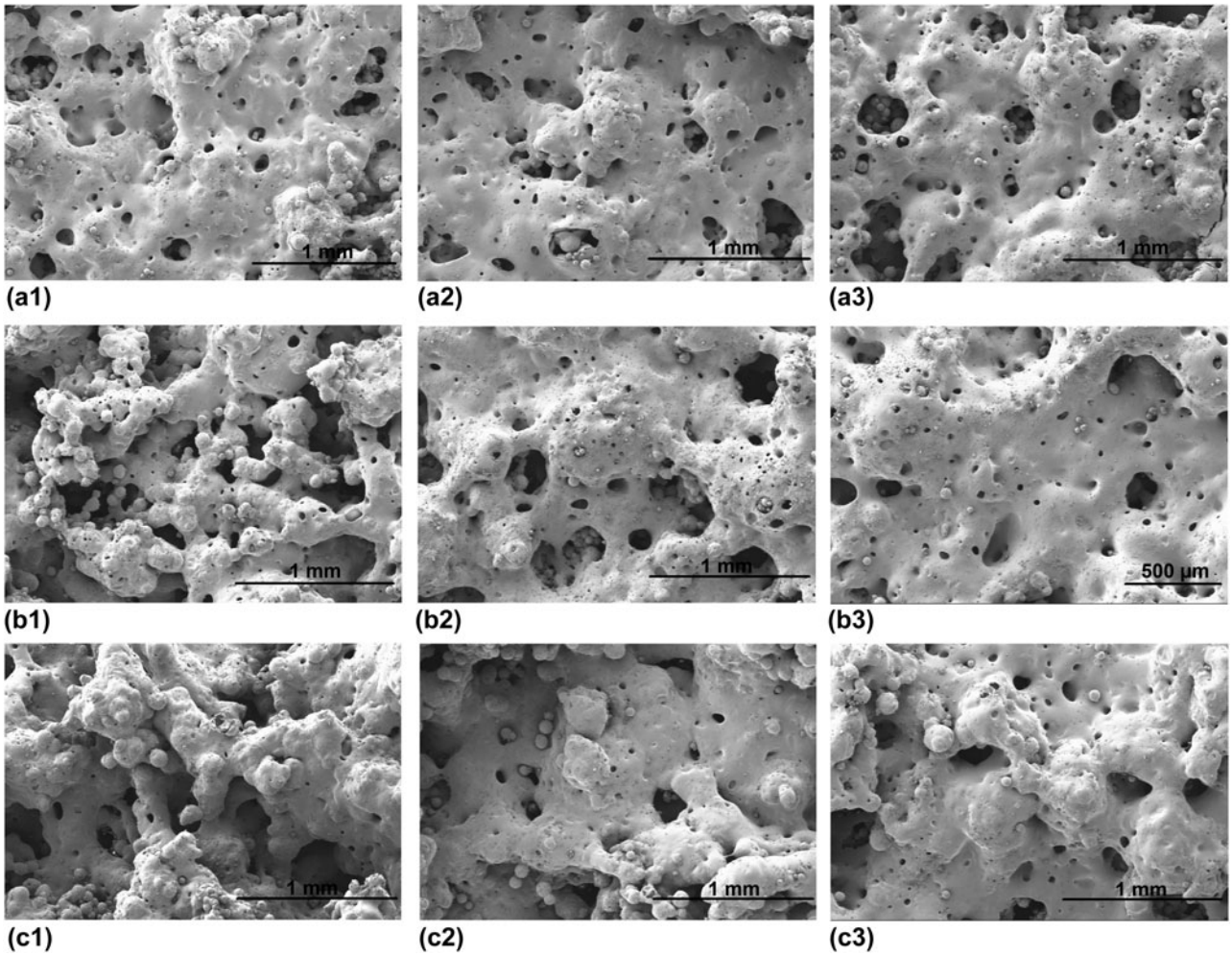



FIG. 6. SEM photographs of sintered PMMA + β-TCP composites with varying process parameters with power settings in the higher ranges. (a1) $P$ = 37.2 W, $s$ = 711 mm/s; (a2) $P$ = 39.6 W, $s$ = 762 mm/s; (a3) $P$ = 42 W, $s$ = 812 mm/s for ED = 0.1 J/mm$^2$. (b1) $P$ = 37.2 W, $s$ = 635 mm/s; (b2) $P$ = 39.6 W, $s$ = 655 mm/s; (b3) $P$ = 42 W, $s$ = 736 mm/s for ED = 0.12 J/mm$^2$; (c1) $P$ = 37.2 W, $s$ = 457 mm/s; (c2) $P$ = 39.6 W, $s$ = 482 mm/s; (c3) $P$ = 42 W, $s$ = 508 mm/s for ED = 0.14 J/mm$^2$.

https://doi.org/10.1557/jmr.2014.211 Published online by Cambridge University Press

uncontrolled porosity levels, as evident from Fig. 7(a). Secondly, excessive laser energy levels can result in extremely high temperatures leading to polymer pyrolysis, which manifests itself in increased porosity levels.[34] Further, with excessive energy input, gases are trapped in the diffused material matrix, driven by the dissolution occurring under the Laplacian excess bubble pressures according to Henry's Law,[27] especially as the viscosity of the matrix decreases. This is evident in regions around closed pores on sectional areas of specimens as shown in Fig. 7(b). With increasing temperature, the bubbles also increase in size due to the pressure and viscosity changes.[32] Eventually, gas pickup, bubble formation and growth, and possible ruptures due to localized explosions give rise to uncontrolled porosity levels depending on the laser power and scan velocity settings. As the PMMA matrix goes through these transformations, the β-TCP particles are in the middle of all this upheaval, generally retarding the freedom of movement, but specifically resulting in relatively lesser viscosity levels. Consequently, the uncontrolled porosity levels due to the gas pickup and bubbling are relatively lesser in specimens sintered using the PMMA + β-TCP composites compared to pure PMMA samples for the same laser settings.

## VI. MORPHOLOGY OF β-TCP PARTICLES IN LASER SINTERED PMMA MATRIX

The dispersion of the β-TCP particles and the consequent composite properties vary with particle size and the overall composition.[35] In this case, the PMMA serves as the biocompatible base matrix while the β-TCP provides the required bioactivity. It is beneficial if the β-TCP particles were dispersed on the surface of the sintered samples so as to promote biological tissue interaction when used as implants or scaffolds for tissue engineering. Figure 8 presents the SEM photographs depicting the dispersion of the β-TCP particles with varying process and material conditions.

As evident from Fig. 8(a), with 10% β-TCP composite, the formation of the base matrix layer improves as the laser power is increased with a given scan speed, reaching optimum quality levels at around 42 W. With this, the PMMA phase is uniformly sintered and fused into a smooth flat layer and the relatively light β-TCP particles float and segregate over the surface. When multilayer samples are generated, this process is likely to continue, with the β-TCP particles occupying the interlayer regions. With further increase in power, at around 45 W, the PMMA layer appears to be bubbling and undulating, and often rupturing, but the β-TCP particles are still segregated over the surface. This dispersion of the β-TCP particles over the surface of the sintered part is expected to increase the bioactivity and the osseoconductivity.[36] According to Kasemo and Lausmaa,[37] biological tissues interact mainly with the outermost atomic layers of an implant. For the growth of bone or to induce osseointegration, the surface of the implant must be conductive, providing direct structural

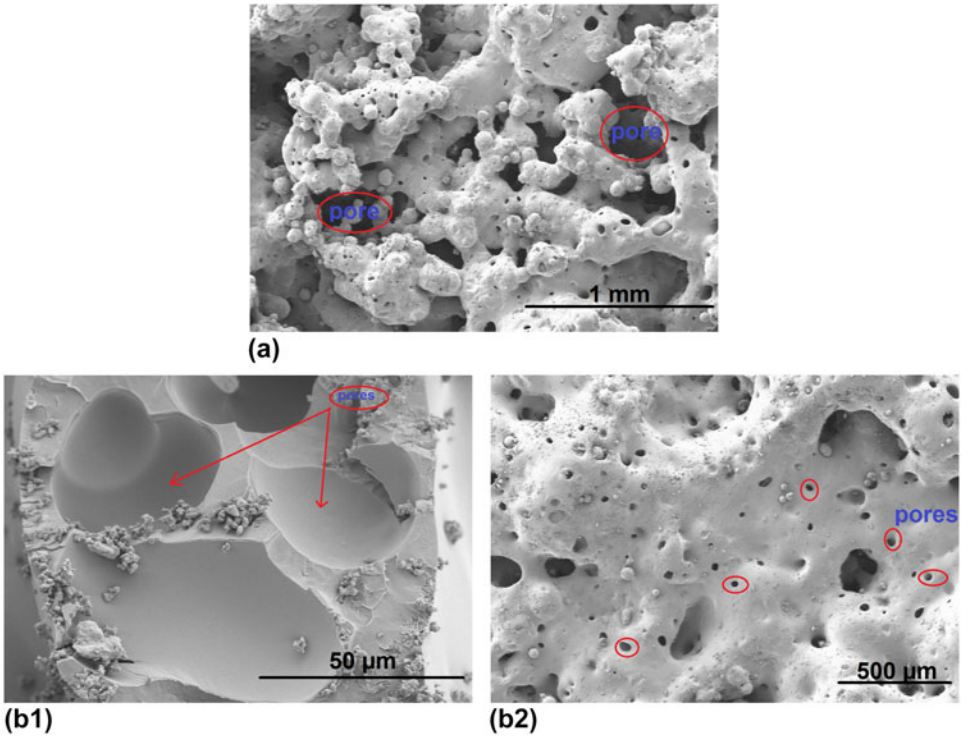



FIG. 7. Uncontrolled porosity in sintered samples (a) resulting from insufficient melting and fusion, and (b1, b2) due to gas pickup.



https://doi.org/10.1557/jmr.2014.211 Published online by Cambridge University Press

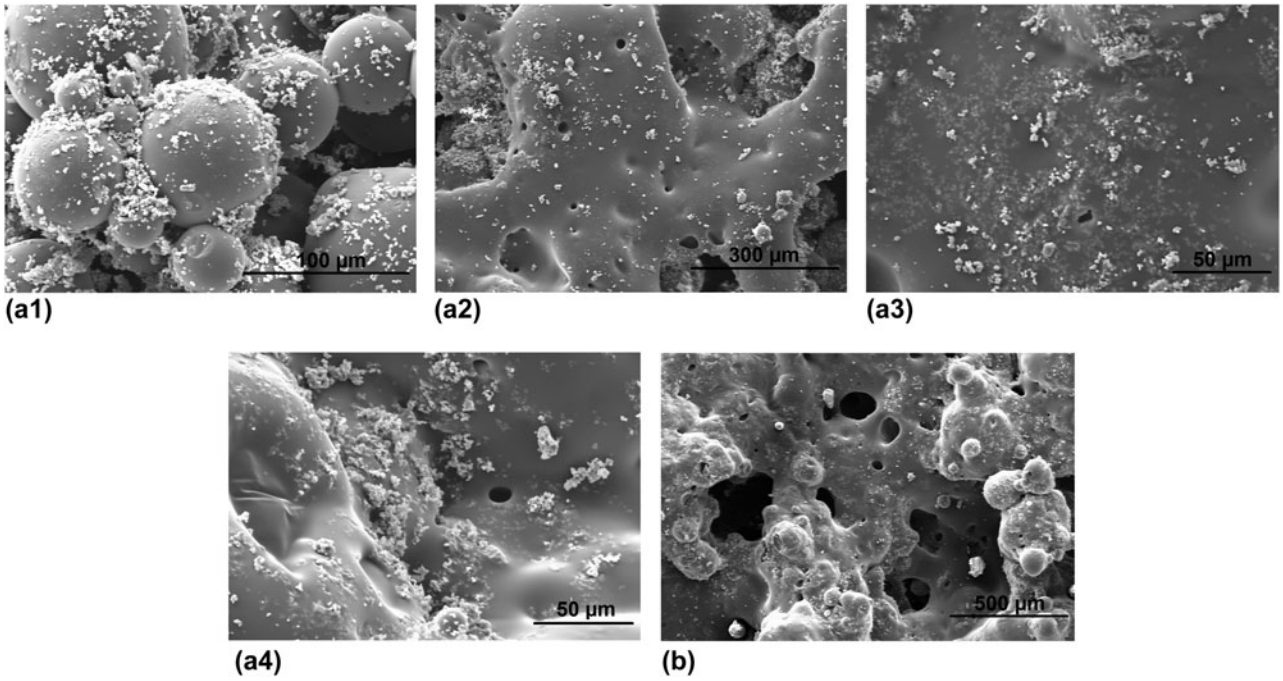



FIG. 8. SEM photographs of sintered layer with 10% β-TCP with varying laser power (a1) 37 W, (a2) 40 W, (a3) 42 W, (a4) 45 W and (b) 20% β-TCP particles.

and functional connections between ordered living bone and the surface of a load-carrying implant, regardless of implantation site, bone quantity and quality, etc.

However, the situation is completely changed with the 20% β-TCP composite, as depicted in Fig. 8(b). While sintering and getting a reasonable sample is difficult, even with the few samples generated, the particle dispersion mechanism appears to have changed completely. The β-TCP particles are fully covered by the PMMA matrix, and the general structure of the layer is very irregular. Apparently, the thermal behavior of the material system appears to have changed in the presence of excessive β-TCP, presumably due to increased absorption of energy as the laser scans a given point and subsequently releases it, eventually resulting in plausible overheating of the PMMA powder. Further, there is increased agglomeration of the β-TCP particles with increased content as against a uniform dispersion of the particles several microns apart as in the case of the lower β-TCP case.

## VII. CROSS-SECTIONS OF THE SINTERED SINGLE-LAYER SAMPLES

The nature of dispersion of the β-TCP particles and the possible agglomeration within the polymer matrix play major roles in determining the final properties of the composite material resulting from laser sintering. Due to incomplete dispersion, a low content of relatively large, unbroken agglomerates can have destructive effects on certain mechanical properties such as tensile and impact strengths and elongation at break.[38] SEM images of the fractured surfaces of the sintered PMMA + β-TCP composite layers presented in Fig. 9 show significant variations. The composite powder consisted of agglomerates of the β-TCP adhering to the PMMA powder. The SLS process, being solely driven by the reduction of surface energy of the base polymer, is unable to overcome the interagglomerate attractive forces and resulted in a mottled microstructure with alternating regions and random distribution of the polymer matrix and β-TCP for a given set of process parameters. Dispersion of the agglomerates depends on their initial dimensions and the mechanism by which they are incorporated into the polymer melt. In the current case, the PMMA and β-TCP powders are mechanically mixed and sintered, resulting in several agglomerates of the β-TCP particles interspersed in the PMMA matrix. The cross-sections show large pores and the dispersion of the β-TCP particles along the boundaries. Comparing the results of Figs. 9(a) and 9(b), it is evident that the higher the β-TCP content, the more the agglomeration of the filler particles along the boundaries of pores, resulting in relatively weak structures.

Scaffolds must possess interconnected open-pore geometries and microstructures permitting cell in-growth and reorganization during the in vitro phase, providing the necessary space for neovascularization from the surrounding tissues in vivo.[39–41] Surface and cross-sectional morphologies of laser sintered PMMA + β-TCP composite

https://doi.org/10.1557/jmr.2014.211 Published online by Cambridge University Press

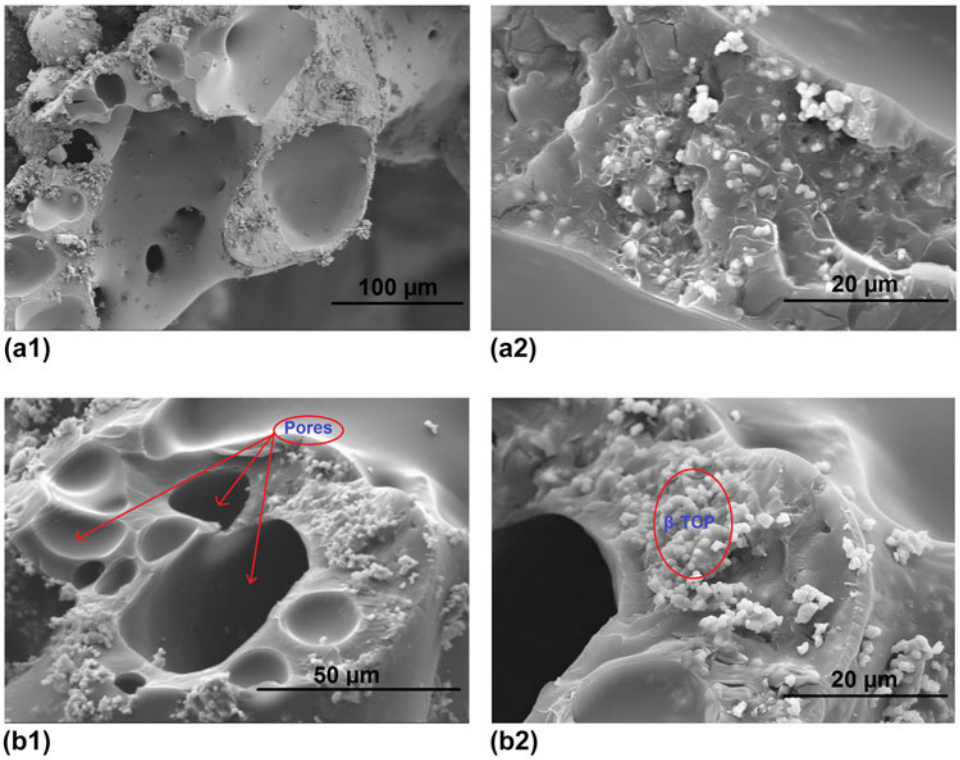



FIG. 9. SEM micrograph of the cross-section of sintered layer (a1, a2) 10% β-TCP and (b1, b2) 20% β-TCP composites.

specimens evaluated in the current research ascertained the presence and controlled variations of porous structures with composition and process parameters. While the presence of the β-TCP altered the responses of the PMMA to laser processing, detrimental effects are observed with excessive amounts. It is evident that controlled sintered structures and mechanical attributes can be obtained through laser sintering of the PMMA + β-TCP composites, but the process parameters and composition need to be optimized considering in vitro and in vivo studies.

## VIII. CONCLUSION

SLS is successfully used to process the PMMA + β-TCP composites to produce single-layer specimens. Laser power and scan speed settings have proved to have profound influences on the interparticle fusion, coalescence, and sintering. Both mechanical properties and porosity levels vary with composition and combinations of process parameters. Morphological variations are noted with the variation of β-TCP from 10% to 20% as the other parameters remain the same. While the agglomeration effects of the filler particles and associated mechanical attributes deteriorate with increasing β-TCP, within allowable limits, the composite material responds well to processing by SLS as evident from the structures of the single-layer test samples produced from the current work. While the PMMA–β-TCP polymer composite is clearly established as a candidate material for processing by SLS, further work is needed that would consider multilayer samples and evaluation of controlled porosities and plausible improvements in osseoconductivities in complex 3D shapes.

## REFERENCES

1. P. Ducheyne, K. Healy, D.E. Hutmacher, D.W. Grainger, and C.J. Kirkpatrick, eds.: *Comprehensive Biomaterials, Vol. 3* (Elsevier, New York, NY, 2011); pp. 257–276.
2. B.D. Ratner, A.S. Hoffman, F.J. Schoen, and J.E. Lemons, eds.: *Biomaterials Science, An Introduction to Materials in Medicine*, 3rd ed. (Elsevier, New York, NY, 2013); p. 1573.
3. F. Barrère, C.A. van Blitterswijk, and K. de Groot: Bone regeneration molecular and cellular interactions with calcium phosphate ceramics. *Int. J. Nanomed.* **1**(3), 317–332 Sep 2006.
4. J.R. Porter, T.T. Ruckh, and K.C. Popat: Bone tissue engineering: A review in bone biomimetics and drug delivery strategies. *Biotechnol. Prog.* **25**(6), 1539–1560 (2009).
5. A.C. Taş, F. Korkusuz, M. Timuçin, and N. Akkaş: An investigation of the chemical synthesis and high-temperature sintering behaviour of calcium hydroxyapatite (HA) and tricalcium phosphate (TCP) bioceramics. *J. Mater. Sci.: Mater. Med.* **8**, 91–96 (1997).
6. M. Kitamura, C. Ohtsuki, S. Ogata, M. Kamitakahara, and M. Tanihara: Microstructure and bioresorbable properties of α-TCP ceramic porous body fabricated by direct casting method. *Mater. Trans.* **45**, 983–988 (2004).
7. J.O. Hollinger and G.C. Battistone: Biodegradable bone repair materials. Synthetic polymers and ceramics. *Clin. Orthop. Relat. Res.* **207**, 290–305 (1986).
8. X. Yu, E.A. Botchwey, E.M. Levine, S.R. Pollack, and C.T. Laurencin: Bioreactor-based bone tissue engineering:

https://doi.org/10.1557/jmr.2014.211 Published online by Cambridge University Press

The influence of dynamic flow on osteoblast phenotypic expression and matrix mineralization. *Proc. Natl. Acad. Sci. U. S. A.* **101**, 11203–11208 (2004).
9. G. Lewis: Properties of antibiotic-loaded acrylic bone cements for use in cemented arthroplasties. *J. Biomed. Mater. Res., Part B* **89B**(2), 558–574 (2009), ISSN: 1552-4973.
10. M. Puska, A. Kokkari, T. Närhi, and P. Vallittu: Mechanical properties of oligomer modified acrylic bone cement. *Biomaterials* **24**(3), 417–425 (2003), ISSN: 0142-9612.
11. B. Flautre, M. Descamps, C. Delecourt, M. Blary, and P. Hardouin: Porous HA ceramic for bone replacement: Role of the pores and interconnections – experimental study in the rabbit. *J. Mater. Sci.: Mater. Med.* **12**, 679–682 (2001).
12. G. Daculsi and N. Passuti: Effect of the macroporosity for osseous substitution of phosphate calcium ceramics. *Biomaterials* **11**, 86–87 (1990).
13. G. Daculsi, N. Passuti, S. Martin, C. Deudon, R.Z. Legeros, and S. Raher: Macroporous calcium-phosphate ceramic for long-bone surgery in humans and dogs clinical and histological study. *J. Biomed. Mater. Res.* **24**, 379–396 (1990).
14. C.P.A.T. Klein, K. de Groot, C. Weiqun, L. Yubao, and Z. Xingdong: Osseous substance formation in calcium phosphate ceramics in soft tissues. *Biomaterials* **15**, 31–34 (1994).
15. M. Descamps, O. Richart, P. Hardouin, J.C. Hornez, and A. Leriche: Synthesis of macroporous b-tricalcium phosphate with controlled porous architectural. *Ceram. Int.* **34**, 1131–1137 (2008).
16. T. Adachi, Y. Osako, M. Tanaka, M. Hojo, and S.J. Hollister: Framework for optimal design of porous scaffold microstructure by computational simulation of bone regeneration. *Biomaterials* **27**, 3964–3972 (2006).
17. S. Saha and S. Pal: Mechanical properties of bone cement; a review. *J. Biomed. Mater. Res.* **18**, 435–462 (1984).
18. W.J. Malony, M.A. Jasty, A. Rosenberg, and W.H. Harris: Bone lysis in well-fixed cemented femoral component. *J. Bone Jt. Surg.* **72B**, 966–970 (1990).
19. I. Ahato: Reverse engineering the ceramic art of algae. *Science* **286**, 1059–1061 (1999).
20. F. Popişter, D. Popescu, and D. Hurgoiu: A new method for using reverse engineering in case of ceramic tiles. *Qual. Access Success* **13**, 409–412 (2012).
21. D. Bombač, M. Brojan, P. Fajfar, F. Kosel, and R. Turk: Review of materials in medical applications. *RMZ – Mater. Geoenviron.* **54**(4), 471–499 (2007).
22. J.M. Williams, A. Adewunmi, R.M. Schek, C.L. Flanagan, P.H. Krebsbach, S.E. Feinberg, S.J. Hollister, and S. Das: Bone tissue engineering using polycaprolactone scaffolds fabricated via selective laser sintering. *Biomaterials* **26**, 4817–4827 (2005).
23. K.H. Tan, C.K. Chua, K.F. Leong, C.M. Cheah, P. Cheang, M.S. Abu Bakar, and S.W. Cha: Scaffold development using selective laser sintering of polyetheretherketone–hydroxyapatite biocomposite blends. *Biomaterials* **24**(18), 3115–3123 (2003).
24. C.K. Chua, K.F. Leong, F.E. Wiria, K.C. Tan, and M. Chandrasekara: Fabrication of poly(vinyl alcohol)/hydroxyapatite in tissue engineering. In *Proceedings of the International Conference on Competitive manufacturing*, World Scientific Publishing Company: Steilhenbosch, 2004.
25. S. Das, S.J. Hollister, C. Flanagan, A. Adewunmi, K. Bark, C. Chen, K. Ramaswamy, D. Rose, and E. Widjaja: Computational design freeform fabrication and testing of Nylon-6 tissue engineering scaffolds. In Rapid prototyping technologies. *Mater. Res. Soc. Symp. Proc.* **758**, 3–5 December 2002, 205–210.
26. N.K. Vail, L.D. Swain, W.C. Fox, T.B. Aufdlemorte, G. Lee, and J.W. Barlow: Materials for bio-medical applications. *Mater. Des.* **20**, 123–132 (1999).
27. L. Hao, M.M. Savalani, Y. Zhang, K.E. Tanner, and R.A. Harris: Selective laser sintering of hydroxyapatite reinforced polyethylene composites for bioactive implants and tissue scaffold development. *Proc. Inst. Mech. Eng. H* **220**, 521 (2006).
28. F. Alessandro, R. Luca: Characterization of laser energy consumption in sintering of polymer based powders. *J. Mater. Process. Technol.* **212**, 917–926 (2012).
29. J.D. Williams and C.R. Dechard: Advances in modelling the effects of selected parameters on the SLS process. *Rapid Prototyping J.* **4**, 90–100 (1998).
30. I. Shishkovsky, Yu. Morozov, and I. Smurov: Nanostructural self-organization under selective laser sintering of exothermic powder mixtures. *J. Appl. Surf. Sci.* **225**, 5565–5568 (2009).
31. J.T. Rimell and P.M. Marquis: Selective laser sintering of ultra high molecular weight polyethylene for clinical applications. *J. Biomed. Mater. Res.* **53**, 414–420 (2000).
32. E. Berry, J.M. Brown, M. Connell, C.M. Craven, N.D. Efford, A. Radjenovic, and M.A. Smith: Preliminary experience with medical applications of rapid prototyping by selective laser sintering. *Med. Eng. Phys.* **19**, 90–96 (1997).
33. B. Caulfield, P.E. McHugh, and S. Lohfeld: Dependence of mechanical properties of polyamide components on build parameters in the SLS process. *J. Mater. Process. Technol.* **182**, 477–488 (2007).
34. N. Woicke, T. Wagner, and P. Eyerer: Carbon assisted laser sintering of thermoplastic polymers. In *Annual Technical Conference – ANTEC, Boston, MA*, 2005.
35. V.M. Khumalo, J. Karger Kocsis, and R. Thoman: Polyethylene synthetic boehmite alumina nanocomposites: Structure, thermal and rheological properties. *Express Polym. Lett.* **5**, 264–274 (2010).
36. L. Di Silvio, M.J. Dalby, and W. Bonfield: Osteoblast behaviour on HA/PE composite surfaces with different HA volumes. *Biomaterials* **23**, 101–107 (2002).
37. B. Kasemo and J. Lausmaa: Surface science aspects on inorganic biomaterials. *Crit. Rev. Biocompat.* **2**, 335–380 (1986).
38. E.K. Sichel and M. Dekker, eds.: *Carbon Black-Polymer Composites: The Physics of Electrically Conducting Composites (Plastics Engineering)*. (Dekker, New York, NY, 1982).
39. J.P. Vacanti, M.A. Morse, W.M. Saltzman, A.J. Domb, A. Perez-Atayde, and R. Langer: Selective cell transplantation using bioabsorbable artificial polymers as matrices. *J. Pediatr. Surg.* **23**, 3–9 (1988).
40. A.G. Mikos, G. Sarakinos, M.D. Lyman, D.E. Ingber, J.P. Vacanti, and R. Langer: Prevascularization of porous biodegradable polymers. *Biotechnol. Bioeng.* **42**, 716–723 (1993).
41. B.D. Boyan, T.W. Hummert, D.D. Dean, and Z. Schwartz: Role of material surfaces in regulating bone and cartilage cell response. *Biomaterials* **17**, 137–146 (1996).

https://doi.org/10.1557/jmr.2014.211 Published online by Cambridge University Press